Concentric ring patterns in needle–plate exploding systems

2007 J. Phys.: Condens. Matter 19 016009

(http://iopscience.iop.org/0953-8984/19/1/016009)

INSTITUTE OF PHYSICS PUBLISHING JOURNAL OF PHYSICS: CONDENSED MATTER

J. Phys.: Condens. Matter **19** (2007) 016009 (9pp) doi:10.1088/0953-8984/19/1/016009

Concentric ring patterns in needle–plate exploding systems

Vandana and P Sen[1]

School of Physical Sciences, Jawaharlal Nehru University, New Delhi-110067, India

E-mail: psen0700@mail.jnu.ac.in

Received 12 September 2006, in final form 16 November 2006
Published 7 December 2006
Online at stacks.iop.org/JPhysCM/19/016009

Abstract

Concentric ring patterns are shown to evolve in an iron metal plate during a single electro-explosion event in the needle–plate configuration. Comparing various materials we show that the input power and its dissipation through the metal plate play a vital role in ring formation. From results obtained by varying the plate and needle voltage polarity, we discuss conditions for their appearance in addition to their dependence on plate material properties.

(Some figures in this article are in colour only in the electronic version)

1. Introduction

Electro-explosion is a phenomenon in which a very high current, suddenly applied to a thin conducting wire, causes it to fragment [1] with concomitant explosion. In an earlier publication [2], we have established electro-explosion in the needle–plate geometry and shown nanoscale modification of a metallic surface during reorganization of the metal plate. This reorganization was initiated through electro-explosion, a nonequilibrium process.

Nonequilibrium processes, however, lead to pattern formation. Patterns are observable macroscopic ordering in a large system arising as a result of interaction amongst its constituent microscopic elements. Being a universal phenomenon, pattern formation continues to draw widespread attention encompassing biological, chemical, hydrodynamical and nonlinear optical systems. Patterns have been observed in fluid convection in Rayleigh–Bénard cells, as Turing patterns in morphogenesis, from instabilities in periodically vibrated liquids (Faraday instability), in vibrated granular media, from avalanches in electrical discharge in gases and in light intensity aggregation from nonlinear response to light passing through a medium. Concentric ring patterns are extremely rare. In a circular domain, roll patterns as a set of concentric rings have only been reported in Rayleigh–Bénard cells, in vertically oscillated fluids and a planar barrier gas discharge system [3].

[1] Author to whom any correspondence should be addressed.

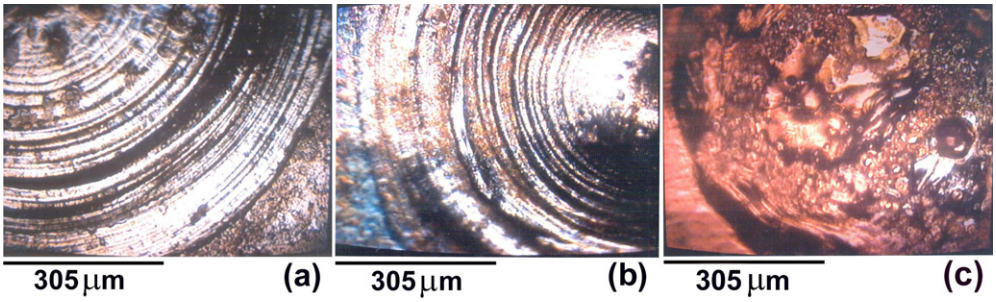

Figure 1. Optical micrographs showing results from explosions in the needle–plate configuration (plate-positive, see text). (a) Fe/Fe_{370p} system, voltage = 48 V; (b) W/Fe_{140p} system, voltage = 48 V; (c) Cu/Cu_{180p} system, voltage = 48 V.

Pattern formation in metals is rare. Patterns have, however, been seen in ion irradiation and sputtered surfaces [4], dendritic growth [5] and electrochemical dissolution of metals [6]. These are typical of problems in pattern formation that take place far from equilibrium.

In this paper, we show the evolution of micron-scale patterns over and above the nanoscale reorganization of the metallic surface. This is achieved by changing the relative polarity of the needle and plate during explosion. We show that the input power and its dissipation play a major role during the entire process. Comparing various materials with different melting point and electron–phonon coupling, we discuss the details of the energy dissipation process and its contribution towards pattern formation. Finally, we discuss the influence of plate polarity on ring formation.

2. Experimental arrangement

The reported single wire single explosion (SWSE) experiments were carried out using Fe, Cu, W, Al, Ag and Ni polished metal plates and tips in the needle–plate geometry. The various experimental details pertaining to SWSE experiments have already been published [2]. The experimental arrangement and the various controls employed to achieve such an experiment have also been shown in this reference.

3. Electro-explosion-induced ring patterns

In figures 1(a) and (b), we show optical micrographs of SWSE results from exploding Fe (diameter = 370 μm) and W tips (diameter = 140 μm) on a Fe plate while holding the plate with a positive polarity (48 V) compared to the needle (hereafter referred to as Fe/Fe_{370p} and W/Fe_{140p} systems; p stands for plate-positive case). The figures clearly show rings emanating from the point of contact made by the respective tips with the Fe plate. The rings die out at the extreme of a circle whose diameter for the Fe/Fe_{370p} system is 1425 μm and for the W/Fe_{140p} system is 1250 μm. As ring patterns are observed in the Fe plate in both cases, it is concluded that ring formation is independent of the wire material.

In figure 2, we show a plot of the current flowing through the needle–plate configuration during the explosion event for the Fe/Fe_{370p} system and the W/Fe_{140p} system. The evolution of current plot is similar in figures 2(a) and (b). The electro-explosion process is accompanied by emission of visible light (red-orange part of the visible spectrum for the Fe/Fe system). An optical micrograph showing plasma formation during explosion in our geometry for the Fe/Fe system is shown as an inset to figure 2(a).

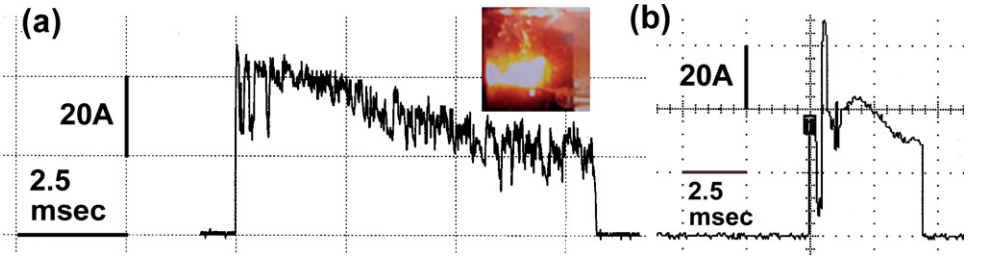

Figure 2. Time evolution of current through the needle–plate configuration during explosion (plate-positive) (a) Fe/Fe_{370p} system, voltage = 48 V; (b) W/Fe_{140p} system, voltage = 48 V. These plots are reproduced from an oscilloscope output in the form of a chart; hence scales are marked manually in each one. In the inset to (a) we show an optical micrograph record of plasma formation during explosion in our geometry for the Fe/Fe system.

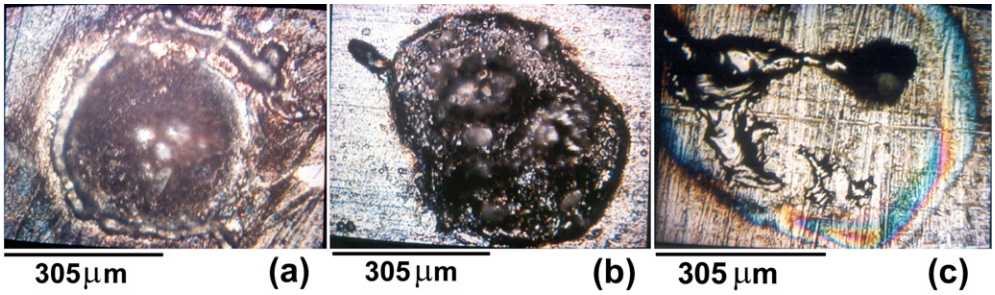

Figure 3. Optical micrographs showing results from explosions in the needle–plate configuration (plate-positive). (a) W/Ag_{100p} system, voltage = 48 V; (b) W/Al_{100p} system, voltage = 48 V; (c) W/W_{100p} system, voltage = 48 V.

Comparing figures 2(a) and (b), we can see that the basic process steps are similar but the energy deposited is likewise reduced with reduction in wire diameter, resulting in a total connect time of 8.25 ms for the Fe/Fe_{370p} system and 4.5 ms for the W/Fe_{140p} system.

4. Dependence of concentric ring formation on plate material

To study the dependence of ring formation on plate material properties, we have performed experiments using other metals. Figures 1(c) and 3 show optical micrographs of SWSE results (plate-positive, 48 V) for the Cu/Cu_{180p}, W/Ag_{100p}, W/Al_{100p} and W/W_{100p} systems.

Figures 1(c) and 3 show that clear concentric ring patterns are not always observed in the metal plate even when all other conditions remain unchanged, namely, voltage conditions. It would thus be reasonable to assign this behaviour to properties of the plate and wire material. However, in figures 1(a) and (b) we have already demonstrated that ring formation does not depend on the wire material. These experiments thus allow us to assign ring formation to properties of the plate material.

4.1. Fe and Cu comparison

As soon as current flows in the circuit, electrons enter the plate electrode. The metallic lattice interacts with these electrons and dissipative energy loss occurs. We call this the first energy coupling to the lattice. This electron–lattice scattering energy initiates melting at the needle–plate contact, vapourization (seen as a dip in the current around 100 μs in figure 2(a)) and thus

expansion of the lattice, reducing the atomic density. During the expansion phase, the voltage remains small but the current increases through the wire due to the formation of a plasma discharge (ionized metal atoms created due to electrons of sufficient energy now available in the state of reduced atomic density) around the partially vapourized wire needle–plate interface region and transfer of current from the neutral wire to the plasma [7].

This expansion and voltage collapse is followed by self-induced magnetic compression in what is now a moving cylindrical plasma column, known in the literature as a Z-pinch [8]. The compressive shock produces plasma velocities of the order of 10 cm μs^{-1}, recorded by other workers [9]. If this velocity is converted to energy for a system such as Fe, we obtain energies in the range of 0.01 MeV. This energy, however, is associated with the plasma group velocity, akin to drift velocity associated with transport electrons in a conductor. As the individual electrons in the electron drift have velocities several orders of magnitude higher than the drift velocity, it is likely that individual ions in the plasma would behave similarly. Our estimate of this energy is several MeV, whereby the de Broglie wavelength associated with the ions is comparable with those of the conduction electrons in the metal. This will allow the ions to transfer energy to the electrons first, followed by energy coupling to the lattice atoms through electron–electron and electron–phonon coupling. We can call this the second energy coupling, and the energy loss is similar to S_e (or $(dE/dx)_e$ where e refers to the electronic manifold), observed in high-energy heavy-ion irradiation. The second energy coupling through high-energy particles induces light emission. There is indeed evidence of high-energy x-ray emission from exploded wire plasmas [10]. During our experiment we have been able to record light in the visible region; this is shown as an inset to figure 2(a). In figure 4 we provide a flow diagram elucidating the sequence of events leading to the various energy transfers that take place starting from the moment of needle and plate contact.

According to ion irradiation experiments, the electron gas energy is coupled to the lattice through electron–electron and electron–phonon coupling [11]. The temperature of the electronic system increases during a time equivalent to the deposition time (10^{-15} s). Following this, the lattice temperature increases mainly because of electron–phonon interaction. The maximum lattice temperature is reached, when both systems are in equilibrium. In our experiment, current flows for milliseconds. So after a time equal to the deposition time, the lattice temperature increase is mainly achieved due to electron–phonon interaction, i.e. for $\sim 10^{-3}$ s.

Sensitivity to electronic energy loss (the second energy coupling in our system) depends on the melting point and the electron–phonon coupling in the system under consideration [12]. The sensitivity is higher for metals having low melting point and high electron–phonon coupling. The two metals Fe and Cu have different behaviour because one belongs to the transition metal series while the other is a noble metal. In our experiments, we obtain distinct and clearly visible rings in Fe while they are absent in Cu. This occurs at the end of the second energy transfer when the compressive shock gives way to an explosive shock [9] leading to pattern formation (figure 4).

The observed result for Fe and Cu (figure 1) is explained based on scaling of the energy deposited to the lattices as a result of electron–phonon coupling. It is known from ion irradiation studies that the lattice temperature in the core of an ion track can reach up to 500 K in noble metals, whereas in transition metals with a strong electron–phonon coupling the core temperature may reach up to 5×10^4 K [13]. Electron–phonon coupling in Fe is higher than in Cu. So Fe is sensitive to electronic energy loss and Cu is insensitive [13] as far as the effect on the lattice is concerned. The values of electron–phonon coupling are 49.8×10^{11} W cm^{-3} K^{-1} for Fe and 4.94×10^{11} W cm^{-3} K^{-1} for Cu (taking $z = 2$) [12]. The values of electrical conductivity are 102.987 (mΩ cm)$^{-1}$ for Fe and 595.8 (mΩ cm)$^{-1}$ for Cu (table 1).

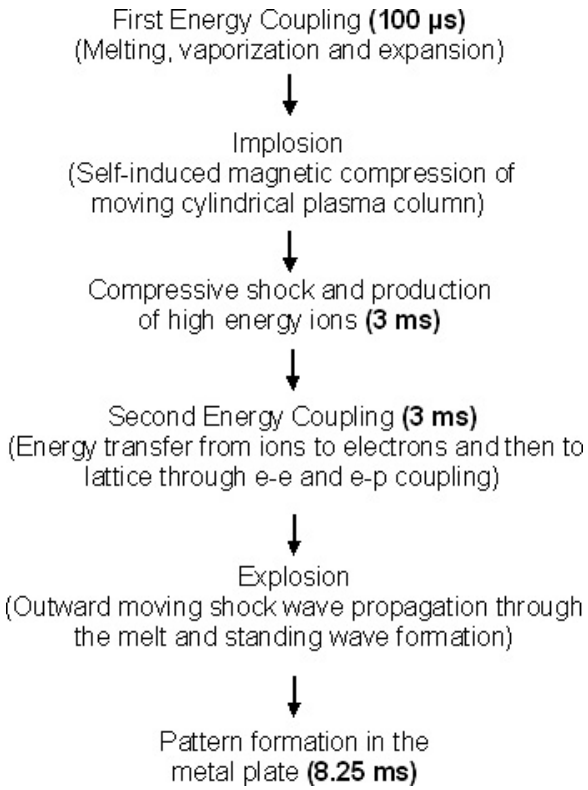

Figure 4. A flow diagram shows the steps leading to concentric ring pattern formation in a metal plate following explosion in the needle–plate geometry. Time markers are introduced in this figure next to the steps. The marker for the first energy coupling is based on data presented in figure 2(a). The other markers are scaled from theoretical estimates given by Lee *et al* [9], to fit the first marker position.

Table 1. Data for several metals used for the description of S_e sensitivity.

Metal	Atomic no.	Density (g cm^{-3})	Heat of vaporization (kJ mol^{-1})	Melting point (K)	Electron–phonon coupling ($\times 10^{11}$) (W cm^{-3} K^{-1})	Heat of atomization (kJ/mol atoms)	Thermal conductivity (J/m s deg)	Electrical conductivity (mΩ^{-1} cm^{-1})
Iron	26	7.86	349.60	1808.2	49.8	418	72.8	102.987
Nickel	28	8.90	370.40	1726.2	40.5	430	90.9	146.199
Tungsten	74	19.3	824.0	3683.2	12.4	849	173	176.991
Aluminium	13	2.702	293.40	933.57	8.14	326	237	376.676
Copper	29	8.96	300.30	1356.6	4.94	338	401	595.8
Silver	47	10.5	250.580	1235.1	1.26	284	429	630.5

Comparing our experiment with ion irradiation experiments, we can say that even if the same amount of energy is deposited in the electronic subsystem in Fe and Cu, the input power dissipation in the metal plate depends mainly on two quantities, electron–phonon coupling and electrical conductivity. In Fe, electron–phonon coupling is larger as compared to Cu, so energy deposited in the metal plate by the high-energy ions is quickly shared primarily among the electron gas by electron–electron interaction in Cu, due to larger electrical conductivity,

whereas in Fe a large part is transferred to the lattice due to a considerably larger electron–phonon coupling. Thus, in the Fe metal plate, the electron–phonon coupling effect dominates over electrical conductivity. Hence the dissipated power is used in melting the plate material more effectively in Fe and not in Cu. So during the spark, a molten phase is easily formed in Fe as compared to Cu. Therefore shock waves propagating through the melt are not able to initiate standing wave formation in Cu, which results in an absence of concentric ring patterns.

In support of this explanation we performed experiments using Al, Ag and W metal plates. The current evolution plots are similar in all cases. But concentric ring patterns were not seen in any of these (figures 1(c) and 3). From table 1, we see that the melting points for Ag, Cu and Al are smaller than for Fe, whereas for W it is larger than for Fe. On comparing electron–phonon coupling data, the metals are ordered as Ag $<$ Cu $<$ Al $<$ W $<$ Fe.

We discussed above that the energy supplied to the electron gas is coupled to the lattice through electron–electron and electron–phonon coupling and results in the production of a molten region in the plate. Hence Ag, with a lower melting point than Fe, can be perceived to favour ring formation, but the lower electron–phonon coupling forces the input energy to dissipate via electron–electron interaction and not by electron–phonon interaction. This propensity is also confirmed by the electrical conductivity values (table 1). The electrical conductivity of W is between that of Fe and Cu, Cu having the largest, while the electron–phonon coupling is between that of Fe and Cu, Fe having the largest. The melting point of W is, however, the highest in the series studied here. All these factors work together and do not allow a molten metal region formation, a prerequisite to ring formation.

Thus a lower melting point and higher electron–phonon coupling favours ring formation. Comparing Al and Cu, the melting point of Al is lower, with a 70% increase in electron–phonon coupling value over Cu. But we still do not generate rings in an Al plate. The electron–phonon coupling values need to be far larger, as will be shown later.

In the experiments reported above, the metal plates can be considered as extremely thick films resulting in the metal bulk acting like a heat sink, disallowing melting of metal surfaces for situations where electron–phonon coupling is low. In order to enhance the effect of a low electron–phonon coupling (whose unit is W cm^{-3} K^{-1}) so as to melt them, the plate thickness needs to be reduced, essentially reducing and isolating the metal atoms where energy is deposited (as one dimension is reduced, W cm^{-3} will increase). In one such experiment with Al thin films, we have been able to generate concentric ring patterns (not reported here).

From our experiments with Al, Ag and W we have been able to explain the absence of concentric ring patterns in Cu. To examine our hypothesis further, we performed an experiment using a metal whose melting point, electrical conductivity and electron–phonon coupling values are close to Fe. This situation exists in Ni and hence we report experiments with a nickel metal plate next. From figure 5, we do not see clear ring formation as in Fe even though melting point and electron–phonon coupling values are similar to Fe. There are rings visible in the outer region, with complex behaviour in the middle. The values of electron–phonon coupling are 49.8×10^{11} W cm^{-3} K^{-1} for Fe and 40.5×10^{11} W cm^{-3} K^{-1} for Ni (taking $z = 2$) [12]. The electrical conductivity values are 102.987 (mΩ cm)$^{-1}$ for Fe and 146.199 (mΩ cm)$^{-1}$ for Ni. We see that the Ni electrical conductivity is larger and the electron–phonon coupling is smaller than those of Fe. This contributes towards complex behaviour in addition to some rings in the outer region. But the presence of rings in the outer region shows that in these experiments, electron–phonon coupling and electrical conductivity play an important role.

5. Dependence of concentric ring formation on plate polarity

To justify that the concentric rings, observed to evolve symmetrically around a metal tip, are not a symmetrical trivial state, we introduce a further instability in the system through a

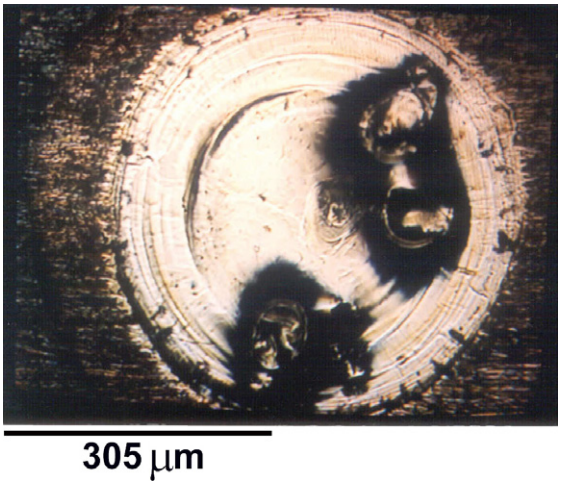

Figure 5. Optical micrograph showing result from explosion in the needle–plate configuration (plate-positive) for the Fe/Ni_{5p} system, voltage = 48 V.

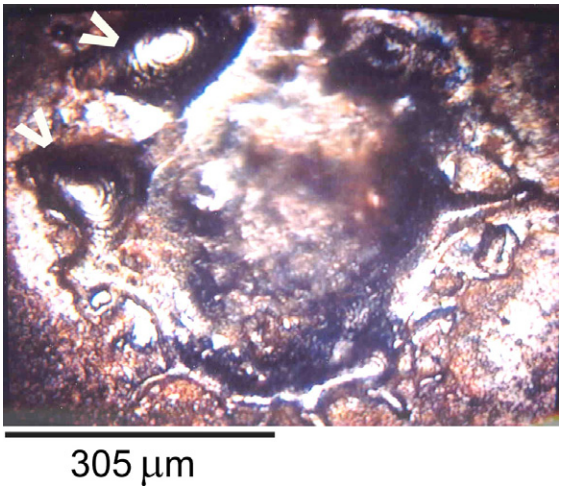

Figure 6. Optical micrograph of the plate after explosion for the W/Fe system in the plate-negative case (see text). Parts of the exploded plate show small rings, marked by white arrows. W tip diameter = 140 μm.

procedure, which involves percolation of current. In figure 6, we show an optical micrograph of SWSE results from exploding a W tip (thickness = 140 μm) on an Fe plate while holding the plate with negative polarity (48 V) compared to the needle (hereafter referred as the W/Fe_{140n} system, n for plate-negative case). The current in this geometry flows from the metal plate to the wire and percolation pertains to current flow through the metal plate, which can be seen as a conductor with infinite diameter when compared to the metal tip.

The result of a percolative nature of current flow is two-fold and can be seen in figure 6. Firstly, no rings are seen to emanate from the needle–plate contact point in the case of a plate-negative situation, and secondly, small regions in the explosion zone are seen to comprise small concentric rings. These regions are indicated in figure 6 with small white arrows.

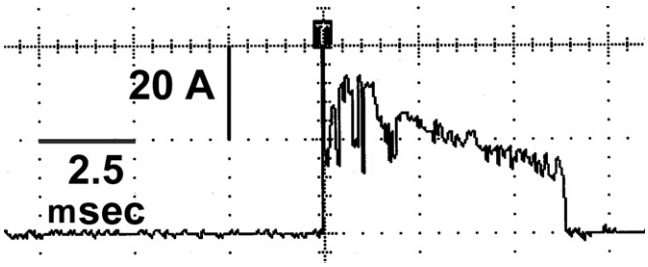

Figure 7. Time evolution of current through the needle–plate configuration during explosion (plate-negative) for the W/Fe_{140n} system, voltage = 48 V. These plots are reproduced from an oscilloscope output in the form of a chart; hence scales are marked manually in each one.

The change in polarity inverts the direction of injection of electrons. Now electrons are moving from the plate to the wire. Unlike before, the electron current density is no longer the same while approaching the needle–plate contact. The plate, being infinitely wide, will in principle supply electrons from its entire width, which is naturally larger than the width of the wire. The reason for this effective width is the percolative nature of current flow in the polycrystalline material of the plate before the electrons enter the wire.

The filamentary nature of the percolative current reduces the effective current density, much required for an efficient explosion. Here self-induced magnetic field compression is not strong enough for shock wave propagation in the plasma region. The total time derivative of the magnetic field is given by

$$(\mathrm{d}B/\mathrm{d}t)_s = (\partial B/\partial t) + v_s\,(\partial B/\partial r)\,,$$

where v_s is the shock velocity and t and r are the time and position coordinates [9]. As the total time derivative depends on partial derivatives of the magnetic field with respect to time and position, for the same Δt, the magnetic field B is required to be of sufficient strength. This acts as a potential barrier for the generation of shock waves. However, some regions reach the current density conditions favouring the formation of rings. This filamentary nature of current flow through the wire in the plate-negative case does not allow for the participation of the entire liquid melt in the formation of rings, easily observed in the plate-positive case (figures 1(a) and (b)).

In figure 7 we show a plot of the current flowing through the needle–plate configuration during the explosion event, for the W/Fe_{140n} system. Comparing figure 7 with figure 2, we see that the basic process remains the same in all plots, but the total connect time is larger for the W/Fe_{140n} system (6.2 ms) as compared to the W/Fe_{140p} (4.5 ms) system and smaller than for the Fe/Fe_{370p} (8.25 ms) system. The longer time taken for current to flow in the case of the Fe/Fe_{370p} system, as compared to the W/Fe_{140n} and W/Fe_{140p} systems, can be explained to be due to larger wire diameter. But the wire diameter is the same for the W/Fe_{140n} and W/Fe_{140p} systems. An explanation of larger connect time in the W/Fe_{140n} system is based on our observation that the energy deposition rate is large in the plate-positive case producing concentric rings which are structures introduced in the plate, hence requiring greater amount of energy, while in the plate-negative case, the energy deposition rate is smaller and hence the plasma survives for a longer time. The modulation on the surface is likewise not as dramatic.

Comparing figures 7 and 2(b), we observe that for the W/Fe_{140n} system, the current takes 1.4 times as long to fall to zero as compared to the W/Fe_{140p} system. Hence the current drop rate (slope) is larger in the W/Fe_{140p} system. Due to the larger slope in the current plot $\partial J/\partial t$, $\partial B/\partial t$ will be larger for the W/Fe_{140p} system as compared to the W/Fe_{140n} system, where

J is the current density. This also supports our observation that the self-induced magnetic field compression is not strong enough for shock wave propagation in the plasma region in the plate-negative situation.

The metal plate region, affected by the explosion in the plate-negative case, is a circle whose diameter for the Fe/Fe_{370n} system is 2950 μm (as compared to 1425 μm for the plate-positive case) while for the W/Fe_{140n} system the value is 2287.5 μm (as compared to 1250 μm for the plate-positive case). These diameters are approximately double those of the plate-positive case, indicating that current filaments originate from a widespread region in the plate when the plate is a source of electrons (plate-negative case).

6. Conclusions

Previous reports of pattern formation in metals essentially indicated diffusion-initiated processes. The technique of electro-explosion in our geometry is new and allows us to introduce nonlinearity in a metal plate and hence induces pattern formation. Our study shows that ring formation in the metal plate depends on the input power dissipation, which is governed by plate metal properties and hence is independent of the wire material. In addition to plate material properties, it depends on the plate polarity. This confirms that concentric rings (symmetrical state) in an iron plate are not trivial, as altered voltage conditions between the needle and the plate force this state to lose stability to a state with lower symmetry even if all other conditions remain the same. With greater understanding, it should be possible to get concentric ring patterns in other metallic systems in this geometry.

Acknowledgments

We thank the University Grants Commission, India, for support under the COSIST programme. One of us (Vandana) thanks the Council for Scientific and Industrial Research (CSIR), India for fellowship. We also thank Dr R Ghosh, School of Physical Sciences, JNU for allowing use of a Tektronix digital storage oscilloscope.

References

[1] Graneau P 1983 *Phys. Lett.* A **97** 253
[2] Vandana and Sen P 2005 *J. Phys.: Condens. Matter* **17** 5327
[3] Gurevich E L, Zanin A L, Moskalenko A S and Purwins H-G 2003 *Phys. Rev. Lett.* **91** 154501 and references therein
[4] Chason E and Aziz M J 2003 *Scr. Mater.* **49** 953
[5] Trivedi R, Liu S and Williams S 2002 *Nat. Mater.* **1** 157
[6] Jaeger N I, Otterstedt R D, Bîrzu A, Green B J and Hudson J L 2003 *Chaos* **12** 231
[7] Duselis P U and Kusse B R 2003 *Phys. Plasmas* **10** 565
[8] Kalantar D H and Hammer D A 1993 *Phys. Rev. Lett.* **71** 3806
[9] Lee K, Kim D and Kim S 2000 *Phys. Rev. Lett.* **85** 3834
[10] Burkhalter P G, Dozier C M and Nagel D J 1977 *Phys. Rev.* A **15** 700
[11] Dufour C *et al* 1993 *J. Phys.: Condens. Matter* **5** 4573
[12] Wang Z G *et al* 1994 *J. Phys.: Condens. Matter* **6** 6733
[13] Seitz F and Koheler J S 1956 *Solid State Phys.* **2** 305